

SUPPLEMENTAL MATERIAL FOR

**Diversity of Organic Components in Airborne Waste Discharged from Sewer
Pipes Repairs.**

Ana C. Morales,¹ Christopher P. West,¹ Brianna N. Peterson,¹ Yoorae Noh,² Andrew J. Whelton,²
Alexander Laskin^{1,*}

¹Department of Chemistry, ²Lyles School of Civil Engineering, ²Department of Environmental and Ecological Engineering, Purdue University, West Lafayette, IN, USA

**Submission prepared for:
Environmental Science: Processes and Impacts**

September 5, 2023

Table of Contents

Supplementary Note 1: <i>Equations used for calculating volatility, viscosity, and molecular metrics of identified species.</i>	3
Supplementary Note 2: <i>Table of selected light absorbing components based on Figure 1 of the main text.</i>	4
Supplementary Note 3: <i>Description of supporting files containing high-resolution mass spectrometry assignments.</i>	7
Supplementary Note 4: <i>APPI(+)-HRMS plots and fractions of the assigned peaks in all HRMS data sets.</i>	9
Supplementary Note 5: <i>Assessment of CHOS species based on the analysis of Kendrick mass defects.</i> ..	11
Supplementary Note 6: <i>Nominal oxidation state of carbon of individual identified waste components, grouped by elemental assignments.</i>	13
Supplementary Note 7: <i>Assessment of plausible structural features based on double bond equivalent values and Van Krevelen diagrams.</i>	14
Supplementary Note 8: <i>Estimation of volatility values of individual molecular components.</i>	17
Supplementary Note 9: <i>Volatility Basis Set Estimation of gas-particle partitioning of waste condensate organic components.</i>	21
Supplementary Note 10: <i>Estimation of glass transition temperature and viscosity values of individual molecular components.</i>	25
Supplementary Note 11: <i>Calibration curves and optical features for selected quantified species.</i>	29
Supplementary Note 12: <i>References.</i>	33

Supplementary Note 1: Equations used for calculating volatility, viscosity, and molecular metrics of identified species.

The volatility, expressed as saturation mass concentration ($\log_{10}C_0$) (C_0 , $\mu\text{g m}^{-3}$) at room temperature, was calculated using the Equation 1 presented in the parameterization approach Li et al. (2016):¹

$$\log_{10}C_0 = (n_C^0 - n_C)b_C - n_O b_O - 2 \frac{n_C n_O}{n_C + n_O} b_{CO} - n_N b_N - n_S b_S \quad (1)$$

Here, n_C^0 represents the reference carbon number, and n_C , n_O , n_N , and n_S represents the number of carbon, oxygen, nitrogen, and sulfur atoms, respectively. Symbols b_C , b_O , b_N , and b_S represent the specific contribution of each atom to $\log_{10}C_0$, as presented by Li et al. (2016).¹ Finally, b_{CO} denotes the carbon-oxygen nonideality presented by Donahue et al. (2011).²

The glass transition temperature and viscosity parameters were calculated using the parameters outlined in DeRieux et al (2018)³ and Equation 2 and 3:

Glass transition temperature (T_g , K):

$$T_g = (n_C^0 + \ln(n_C))b_C + \ln(n_H)b_H + \ln(n_C)\ln(n_H)b_{CH} + \ln(n_O)b_O + \ln(n_C)\ln(n_O)b_{CO} \quad (2)$$

Viscosity (η) (Pa S):

$$\eta = \eta_\infty e^{\frac{T_0 D}{T - T_0}} \quad (3)$$

Where $\eta_\infty = 10^{-5} \text{Pa S}$ (based on Angell 1991)⁴, D is the fragility parameter which is assumed to be 10 (based on DeRieux, et al. 2018)³, and T_0 is the Vogel temperature calculated as

$$T_0 = \frac{39.17 T_g}{D + 39.17}$$

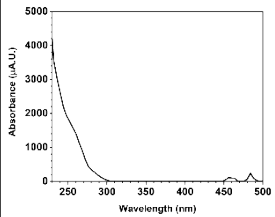
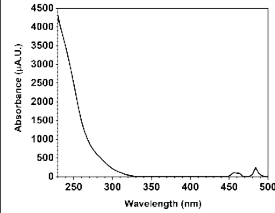
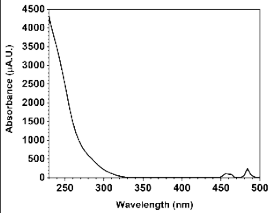
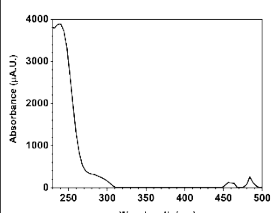
The nominal oxidation state of carbon (NOS_C) values were calculated using Equation 4 from Kroll et al^{5,6} extended to include N and S compounds.⁷

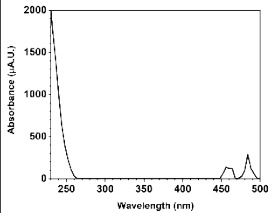
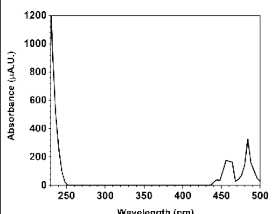
$$\text{OS}_C = 2 \frac{O}{C} + 3 \frac{N}{C} + 2 \frac{S}{C} - \frac{H}{C} \quad (4)$$

Supplementary Note 2: Table of selected light absorbing components based on Figure 1 of the main text.

Table S1. Selected resin components, polycyclic aromatic hydrocarbons, and oxidized polycyclic aromatic hydrocarbons identified by HPLC-PDA-HRMS analysis of waste condensates.

Experimental m/z	Theoretical m/z	Error (ppm)	Mode	Retention Time (min)	Neutral Formula	PDA Record	Description
123.044	123.045	-0.211	ESI(+)	19.11	$C_7H_6O_2$		Benzoic Acid oxidized derivative of styrene and decomposition product of peroxide initiators
107.049	107.050	-0.757	ESI(+)	32.65	C_7H_6O		Benzaldehyde oxidized derivative of styrene and decomposition product of peroxide initiators
225.091	225.092	-0.071	ESI(+) APPI(+)	38.53	$C_{15}H_{12}O_2$		oxidized polycyclic aromatic hydrocarbon

187.075	187.076	-0.289	ESI(+) APPI(+)	39.33	$C_{12}H_{10}O_2$		oxidized polycyclic aromatic hydrocarbon
121.065	121.065	-0.504	ESI(+)	39.42	C_8H_8O		Acetophenone oxidized derivative of styrene and decomposition product of peroxide initiators
105.069	105.070	-0.542	ESI(+) APPI(+)	39.42	C_8H_8		Styrene polymerization monomer
223.112	223.112	-0.009	ESI(+) APPI(+)	47.87	$C_{16}H_{14}O$		oxidized polycyclic aromatic hydrocarbon

202.077	202.078	0.950	ESI(+) APPI(+)	59.20	$C_{16}H_{10}$	 <p>Absorbance (μA.U.)</p> <p>Wavelength (nm)</p>	Pyrene polycyclic aromatic hydrocarbon
276.093	276.094	0.551	ESI(+) APPI(+)	72.71	$C_{22}H_{12}$	 <p>Absorbance (μA.U.)</p> <p>Wavelength (nm)</p>	benzo[<i>ghi</i>]perylene polycyclic aromatic hydrocarbon

Supplementary Note 3: *Description of supporting files containing high-resolution mass spectrometry assignments.*

The following is a copy of the README file included in the supporting datasets included as DOI: 10.4231/TPKM-6075

Datasets for

"Diversity of Organic Components in Airborne Waste Discharged from Sewer Pipes Repairs."

Authors: Ana C. Morales, Christopher P. West, Brianna N. Peterson, Yoorae Noh, Andrew J. Whelton, Alexander Laskin

In this folder, high-resolution mass spectrometry (HRMS) datasets for the samples analyzed are included. The datasets contain different sheets that correspond to the HRMS ionization mode that the ions were detected in, where each row corresponds to a detected ion. The HRMS ionization modes utilized in this study are electrospray ionization (ESI) positive (+) and negative (-) modes, and atmospheric pressure photochemical ionization positive mode (APPI(+)). Two types of resins were used at the installation sites: an S-based resin and a VE-based non-styrene resin. At sites X1, X4, and X5 (, the S-based resin was used. At site X2, the VE based resin was used. Sample names correspond to the sample site. A) m/z: The mass-to-charge ratio of the ion detected by the mass spectrometer.

Each file contains the following information:

- B) Neutral Mass: The neutral mass of the molecule determined after peak assignments.
- C) Peak Intensity: The detected intensity of the ion as reported by the mass spectrometer.
- D) Retention Time (min): The LC retention time in minutes of the detected ion.
- E) Error: The uncertainty of the molecular assignment in parts per million units
- F) C: The number of carbon atoms in the molecule.
- G) H: The number of hydrogen atoms in the molecule.
- H) N: The number of nitrogen atoms in the molecule.
- I) O: The number of oxygen atoms in the molecule.
- J) S: The number of sulfur atoms in the molecule.
- K) Na: The number of sodium atoms in the molecule.

L) DBE: The calculated double bond equivalence value of the neutral molecule based on the assigned elemental formula.

M) Class: Molecular class of the detected species based on the assigned elemental formula.

N) O/C ratio: The ratio of oxygen to carbon atoms.

O) H/C ratio: The ratio of hydrogen to carbon atoms.

P) Aromaticity Index: The calculated aromaticity index value of the molecule based on the assigned elemental formula.

Q) Nominal Oxidation State of Carbon; NOSc: The calculated nominal oxidation state of carbon value for the molecule based on the assigned elemental formula.

R) Glass Transition Temperature; T_g (K): The calculated glass transition temperature in Kelvin based on the assigned elemental formula.

S) Saturation Mass Concentration; logC₀ (μg m⁻³): The calculated saturation mass concentration in micrograms per cubic meter based on the assigned elemental formula.

T) viscosity; η (Pa s): The calculated viscosity in pascal seconds based on the assigned elemental formula.

U) Maximum Carbonyl Ratio: The calculated maximum carbonyl ratio of the molecule based on the assigned elemental formula

The following datasets are included in this folder:

- 1) X1_Master -This file corresponds to sample number X1.
- 2) X2_Master -This file corresponds to sample number X2.
- 3) X4_Master -This file corresponds to sample number X4.
- 4) X5_Master -This file corresponds to sample number X5.

Supplementary Note 4: *APPI(+)-HRMS plots and fractions of the assigned peaks in all HRMS data sets.*

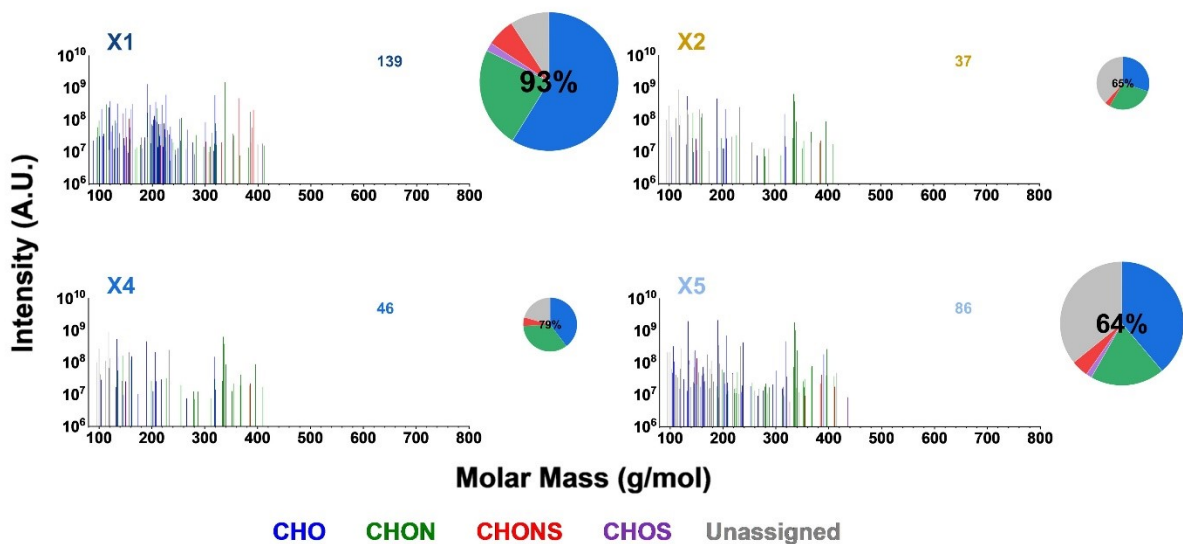


Figure S1. Mass spectra of four waste condensates acquired in *APPI(+)* mode. Assigned peaks are plotted as neutral species, where the x-axis represents the molar mass (g/mol). The pie charts show color-coded relative fractions of different formula categories. Sizes of the pie charts are proportional to the numbers of detected species noted by legends in each panel. The percent values in charts show fractions of the assigned MS peaks in each dataset.

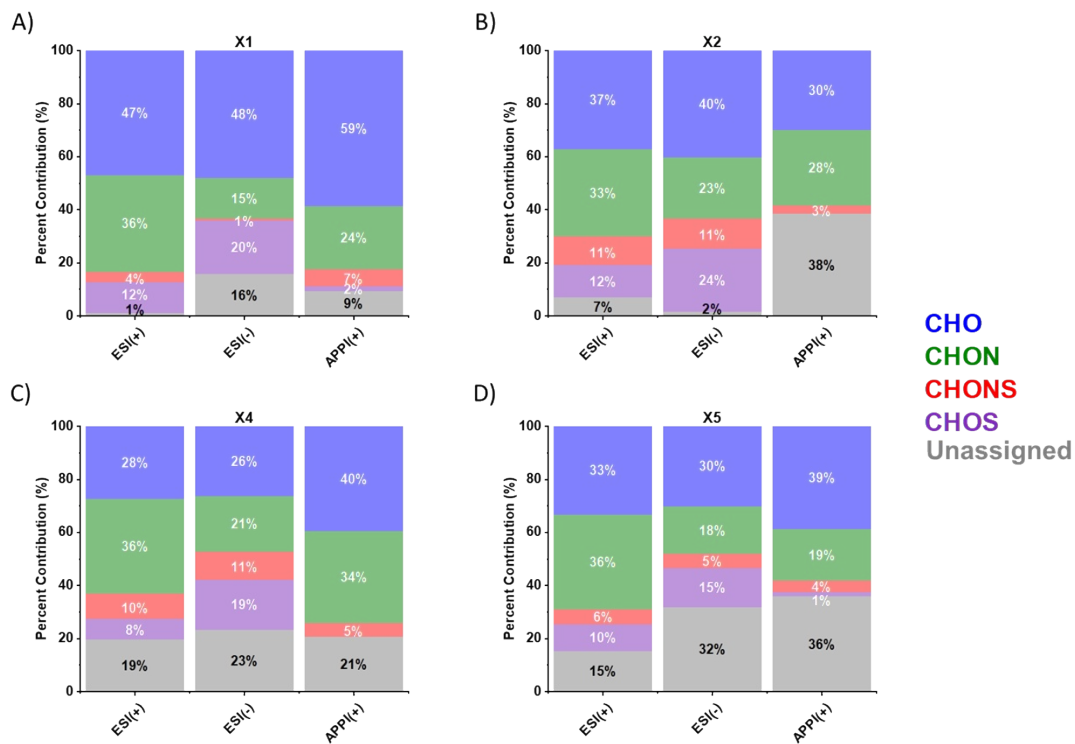


Figure S2. Percent contribution of assigned formula classes based on the total number of assignments per class for each ionization mode. Colors of the bars correspond to the molecular assignments noted in the legends

Supplementary Note 5: *Assessment of CHOS species based on the analysis of Kendrick mass defects.*

CHOS species were investigated using Kendrick mass analysis to determine the different S-containing organic species present in the samples. The plausible organosulfates contain 4 or more oxygen atoms in the neutral formulas ($O/C \sim 0.2-0.5$). The subset $C_nH_{2n+1}SO_{4.9}$ ($DBE = 0; 5 < n < 24$) was present in all four samples and likely represents the saturated organosulfates.⁸ An additional subset $C_nH_{2n-1}SO_{4.7}$ ($DBE < 5; 7 < n < 30$) for low unsaturated organosulfates was also present in X2, X4, and X5. There were many additional CHOS species with a large number of oxygen atoms, such as $C_nH_{2n-13}SO_{4.7}$ ($DBE = 7, 8; 10 < n < 42$), corresponding to species with at least one sulfonate group attached to an oxygen-free substituent, as well as aromatics corresponding to species with high AI indices ($AI > 0.5$).^{9,10}

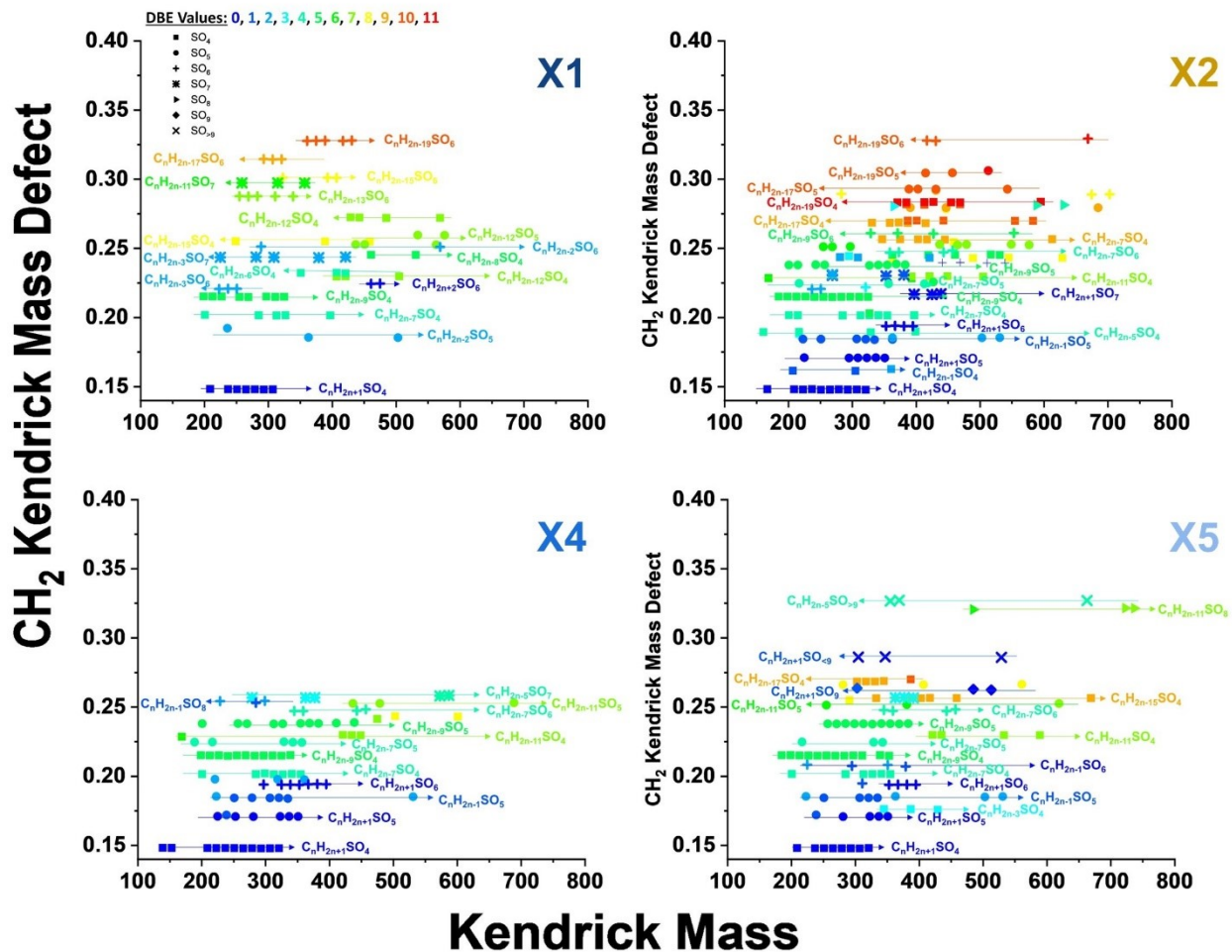


Figure S3. $-\text{CH}_2$ Kendrick mass defect versus Kendrick mass plots for selected organosulfate species. Symbols represent the number of oxygens in the $\text{CHSO}_{4 \rightarrow 9}$ group and are color coded to the DBE of each compound. Representative trends are denoted by the horizontal lines.

Supplementary Note 6: *Nominal oxidation state of carbon of individual identified waste components, grouped by elemental assignments.*

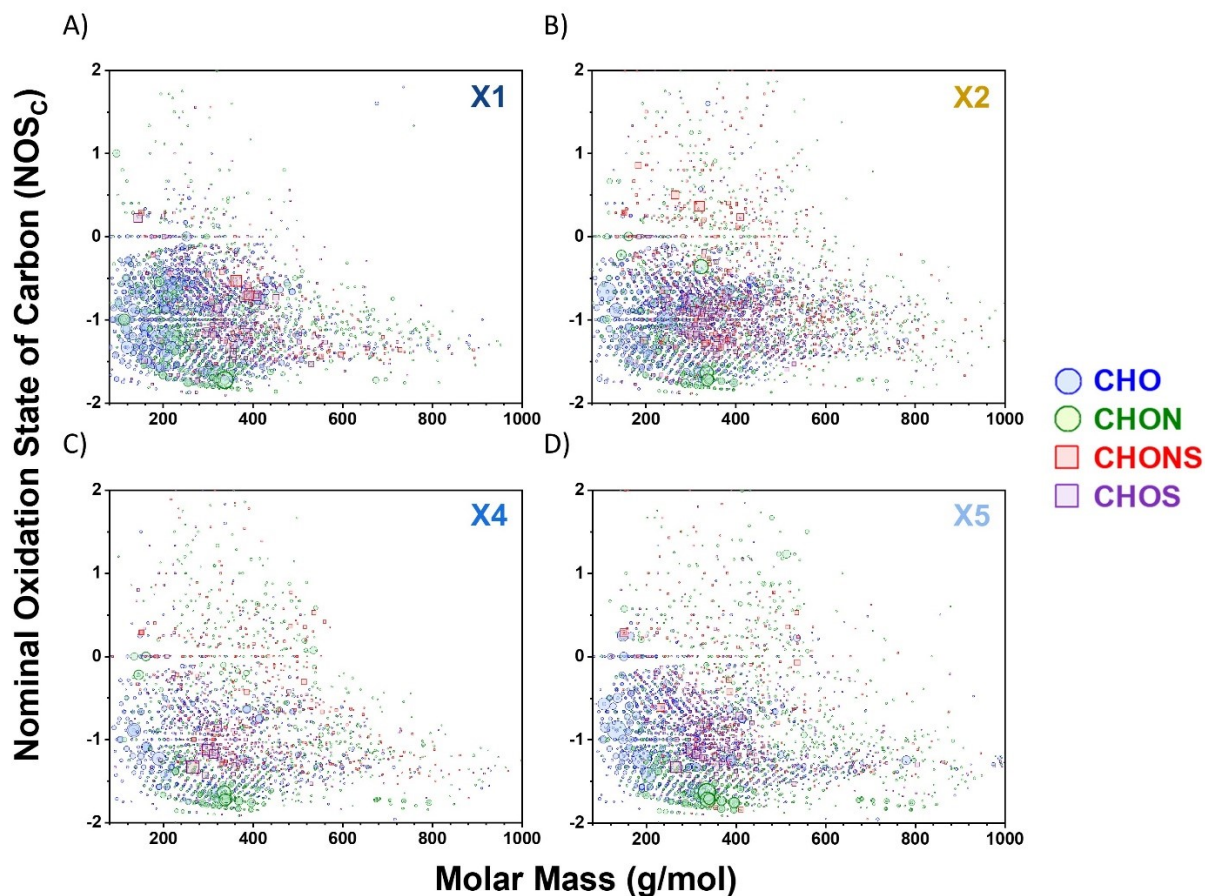


Figure S4. *Nominal oxidation state of carbon (NOS_C) as a function of molar mass. Symbols are color coded to the molecular assignment of neutral formulas in both APPI and ESI modes. Sizes of individual symbols are proportional to the intensity^{1/4} of corresponding MS peaks.*

Supplementary Note 7: *Assessment of plausible structural features based on double bond equivalent values and Van Krevelen diagrams.*

The differences in chemical compositions and structures among the four samples was investigated by plotting the DBE values versus carbon plus nitrogen (C+N) number for the neutral species assigned in each ionization mode (Figure S5). The DBE plots in Figure S5 show a highly complex mixture of both aromatic and aliphatic compounds. Moreover, the chemical classes span the entire molecular size range and fall into both ‘aromatic’ and ‘aliphatic’ regions, further highlighting the complexity of the waste condensates. To better visualize the chemical classes, the Van Krevelen (oxygen to carbon ratio versus hydrogen to carbon ratio) plots are presented in Figure S6. Van Krevelen diagrams are frequently used to quantitatively determine the major chemical species in complex organic mixtures.¹¹

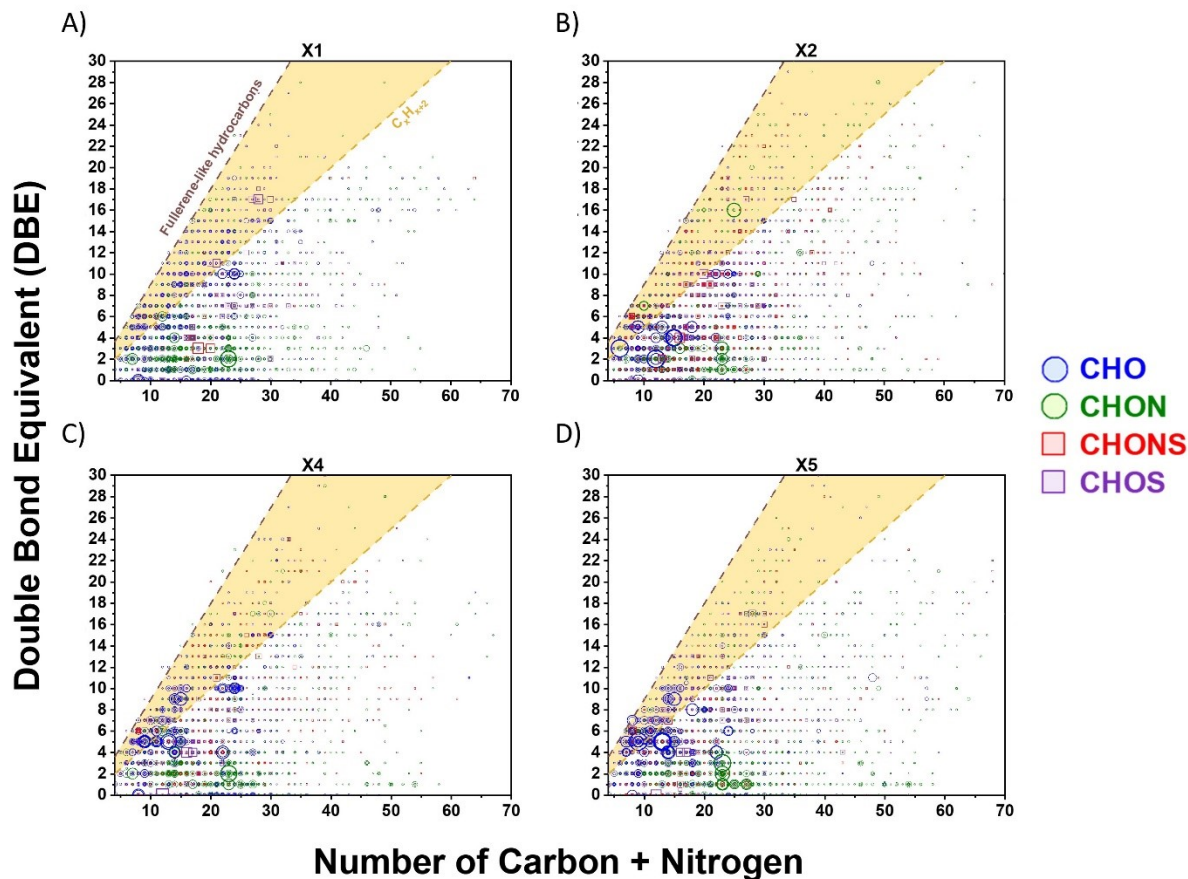


Figure S5. DBE values versus number of carbon plus nitrogen atoms in the assigned species for each CIPP waste condensate. The reference lines indicate DBE values of linear polyenes C_xH_{x+2} with $DBE = 0.5 \times C$ and fullerene-like hydrocarbons with $DBE = 0.9 \times C$, where the shaded area represents likely aromatic compounds.¹² Sizes of individual symbols are proportional to the intensity^{1/4} of corresponding MS peaks. Colors of symbols correspond to the molecular assignments of the neutral formulas inferred from both APPI and ESI modes.

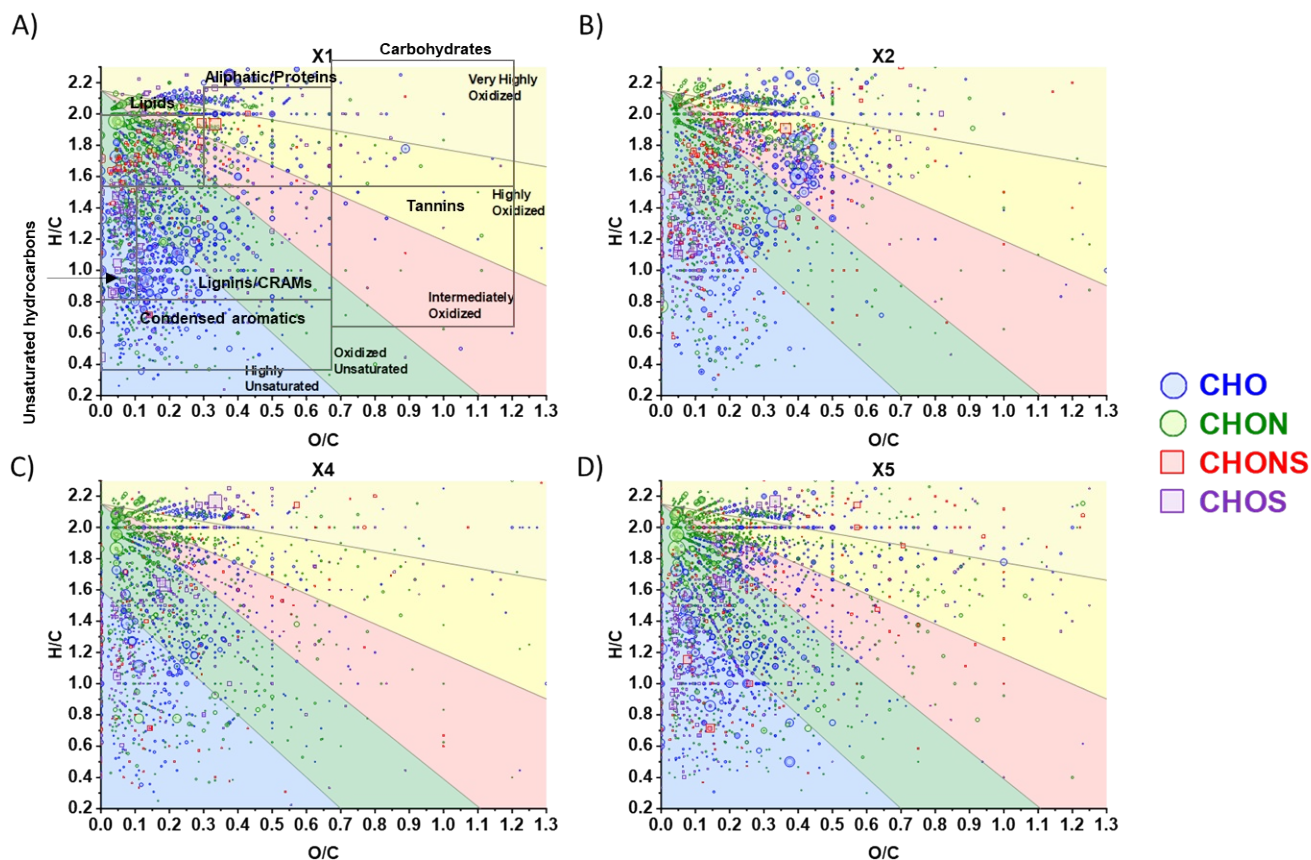


Figure S6. Van Krevelen plot for CIPP condensates. Symbols are color coded to the molecular assignment of neutral formulas in both APPI and ESI modes. Sizes of individual symbols are proportional to the intensity^{1/4} of corresponding MS peaks.

Supplementary Note 8: *Estimation of volatility values of individual molecular components.*

Figure S7 shows the molecular corridor plots depicting the C_0 values of individual components as a function of molar mass for assigned species color-coded by their oxygen to carbon (O:C) ratio. The observed compounds fall in between the upper and lower limiting boundaries represented by linear alkanes (C_xH_{2x+2}) and sugar alcohols ($C_xH_{2x+2}O_x$), respectively. In the waste from the styrene-based sites, many of these compounds contain low O:C ratios and are located closer to the linear alkane line in Figure S7, consistent with the DBE plots, Van Krevelen diagrams, and NOS_C values shown above (Figs S4-S6). Interestingly, the LVOC sample contains the largest total number of ELVOC (39%) and spreads across a wider range between the boundary lines, where the compounds closer to the sugar alcohol line contain higher O:C ratios.

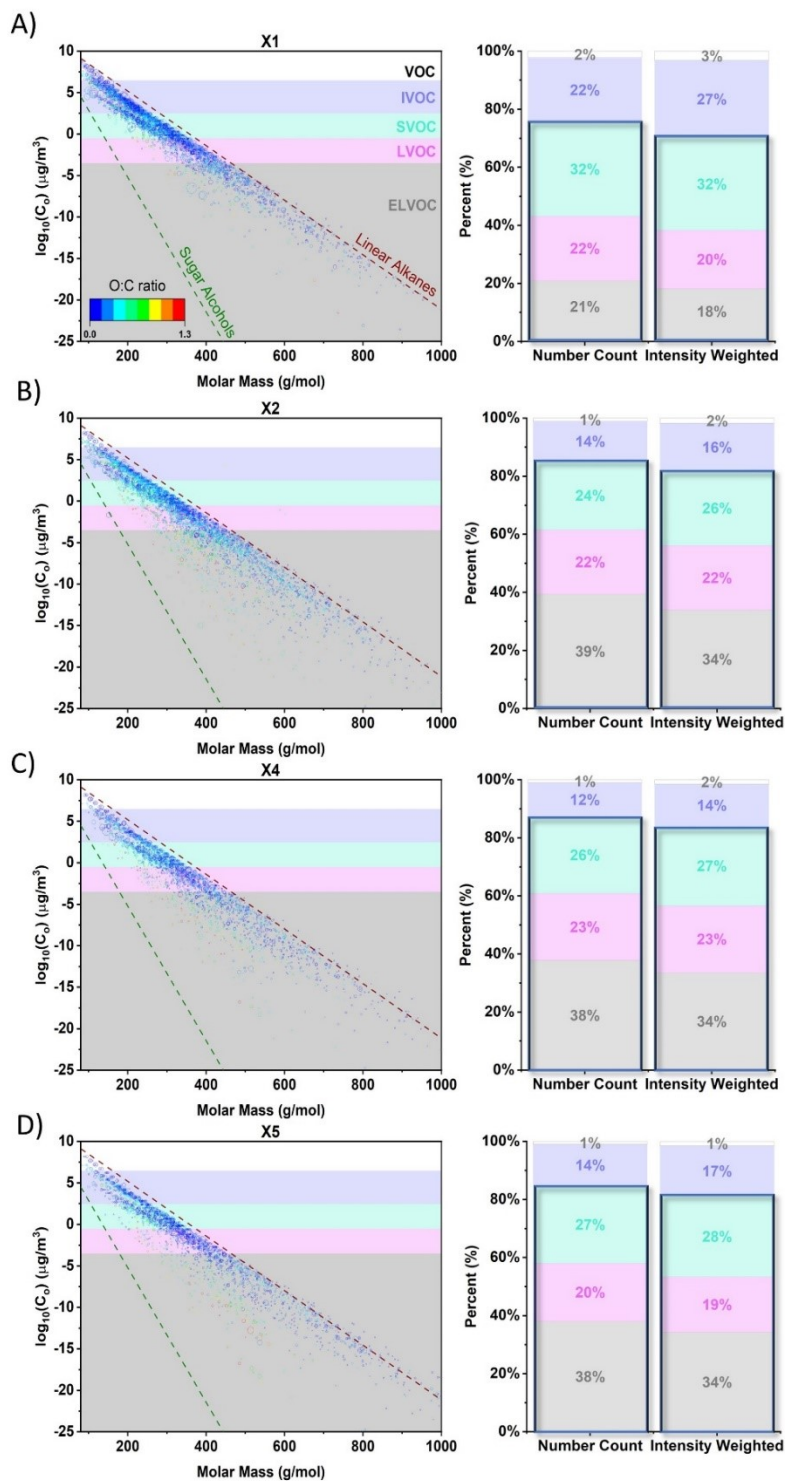


Figure S7. Saturation mass concentration ($\log_{10}C_0, \mu\text{g m}^{-3}$) estimates of individual assigned species in each sample. The background colors indicate the volatility ranges of the organic compounds (OC) reported in Donahue et al. (2012)¹³: from top to bottom, volatile OC (VOC), intermediate-volatility OC (IVOC), semi volatile OC (SVOC), low-volatility OC (LVOC), and extremely low volatility VOC (ELVOC). The reference lines indicate the volatility trends of linear alkanes (dashed red line, top) and sugar alcohols

(dashed green line, bottom). Sizes of individual symbols are proportional to the intensity^{1/4} of corresponding MS peaks. Colors of symbols are proportional to the oxygen to carbon ratio of the neutral formulas in both APPI and ESI modes. Percent contribution of counts and MS intensity of assigned species to volatility class for each CIPP waste condensate are presented on the right side of each plot. Blue boxes represent solid and semi-solid fractions that will contribute to OA mass.

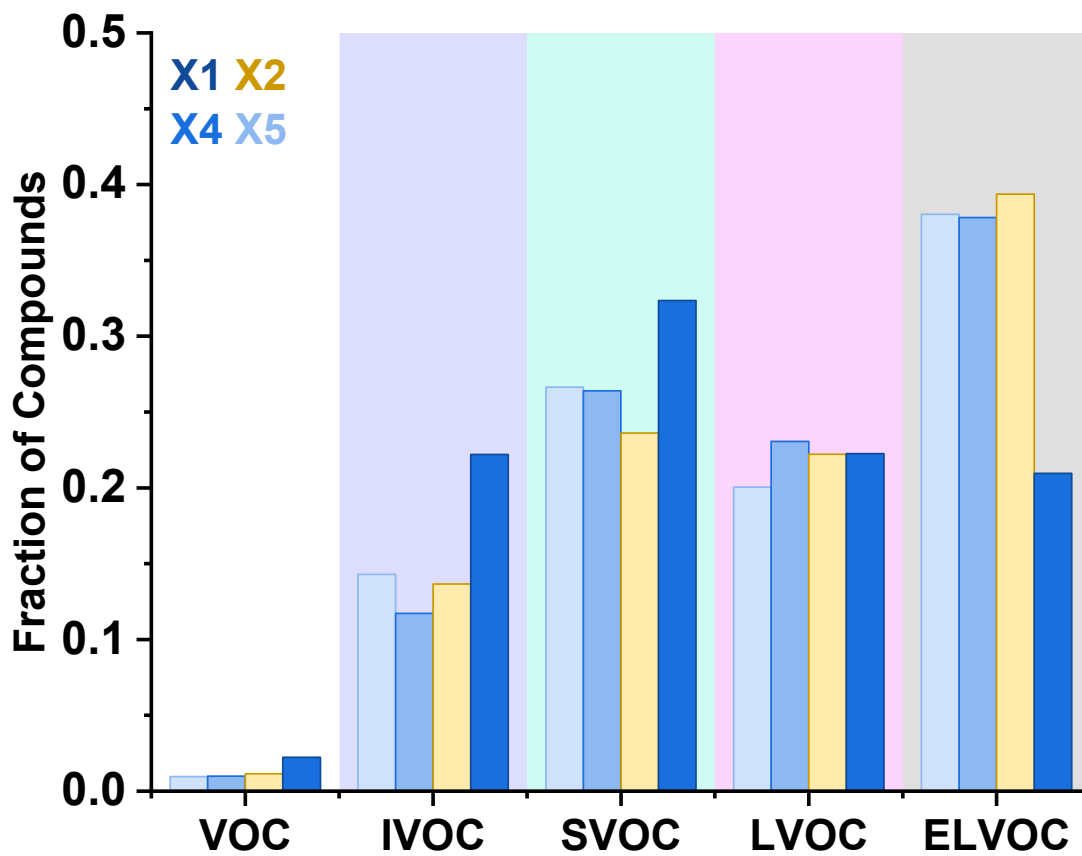


Figure S8. Percent contribution of counts to volatility class for each sample. The background colors indicate the volatility ranges of the organic compounds (OC) reported in Donahue et al. (2012)¹³: from left to right, volatile OC (VOC), intermediate-volatility OC (IVOC), semi volatile OC (SVOC), low-volatility OC (LVOC), and extremely low volatility VOC (ELVOC). Fractions are relative to the total number of compounds detected in each individual sample.

Supplementary Note 9: Volatility Basis Set Estimation of gas-particle partitioning of waste condensate organic components.

Figures S9-S11 show the volatility basis set estimations (VBS)¹⁴ for the four samples at different organic mass loadings (1, 10, and 100 $\mu\text{g m}^{-3}$) to determine if species are present in either the gas phase or particle phase based on the estimated saturation mass concentration. The individual species j are grouped based on their $C_{0,j}$ values (equation 1) into a set of $(\log C^*)_i$ bins i of integer values (e.g., 4, 3, 2 etc., where the integers correspond to the upper bin boundaries). Relative heights (H_i) of bins i are calculated using equation 5

$$H_i = \frac{[\sum_j (I_j \times MW_j)]_i}{\sum_i [\sum_j (I_j \times MW_j)]_i} = \frac{[\sum_j C_{0,j}]_i}{\sum_i [\sum_j C_{0,j}]_i}, \quad \sum_i H_i = 1$$

(5)

The equation assumes a linear relationship between ion intensity I_j and the molar concentration of individual components j , which implies that mass concentration values $C_{0,j}$ are scalable with $I_j \times MW_j$, where MW_j is molecular weight of species j .

The particle-phase mass fractions X_i^p in individual bins i are then calculated for different values of the total organic mass loadings C_{tOM} in the air, e.g., 1, 10, 100, etc. $\mu\text{g m}^{-3}$, using equation 6.

$$X_i^p = H_i \times \frac{C_{tOM}}{C_{tOM} + C_i^*}$$

(6)

Additionally, equations 5 and 6 imply a uniform ESI sensitivity for all individual species. However, ESI sensitivity typically increases between ~ 100 m/z and ~ 300 m/z by a factor of ~ 10 and is dependent on H/C

and O/C.¹⁵ When considering quantitative interpretation of ESI data, we are biased towards species with larger m/z .¹⁵

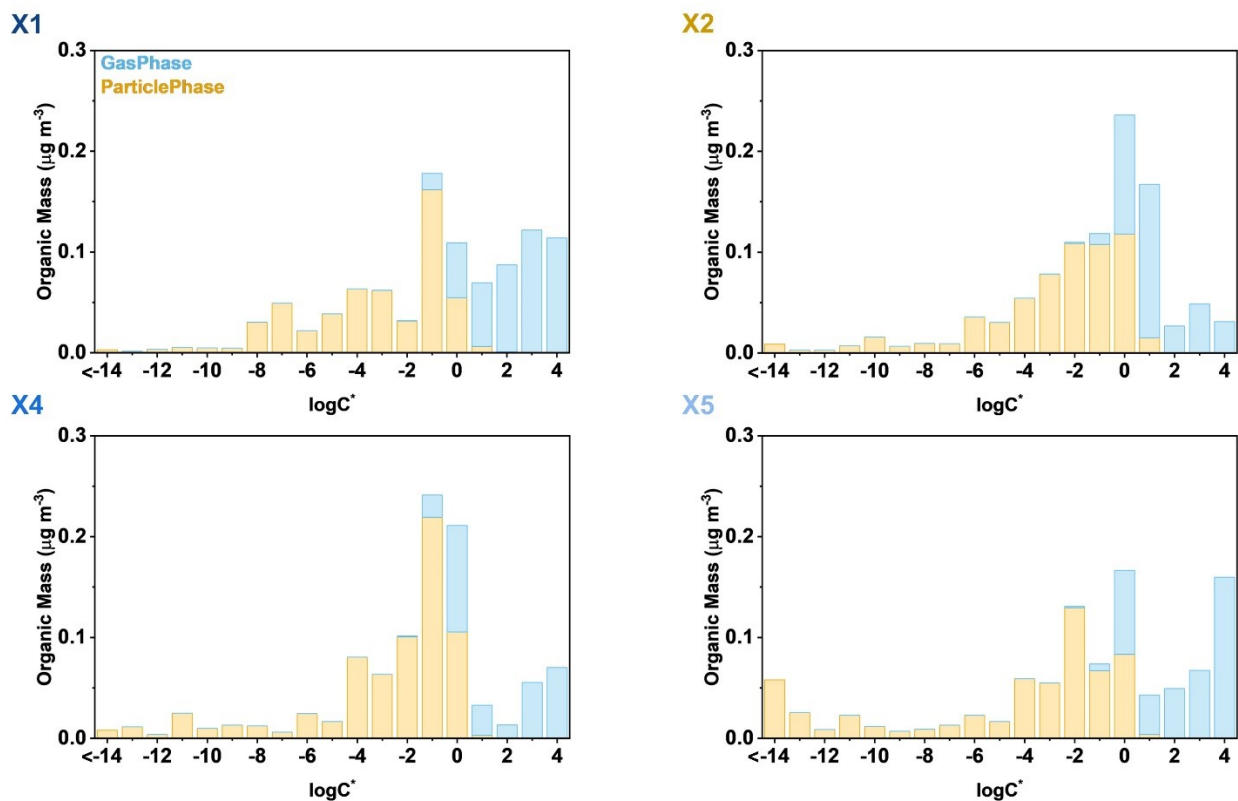


Figure S9. Volatility Basis Set (VBS) plots of organic components identified in the waste condensate samples, calculated for aerosolized mixtures with a total organic mass (OM) loading of $1 \mu\text{g m}^{-3}$. The estimated mass concentrations of individual components (C_i , $\mu\text{g m}^{-3}$) are binned into $\log C^*$ bins of integer values shown on the x-axis. Yellow and blue areas indicate OM fractions in particle and gas phases, respectively.

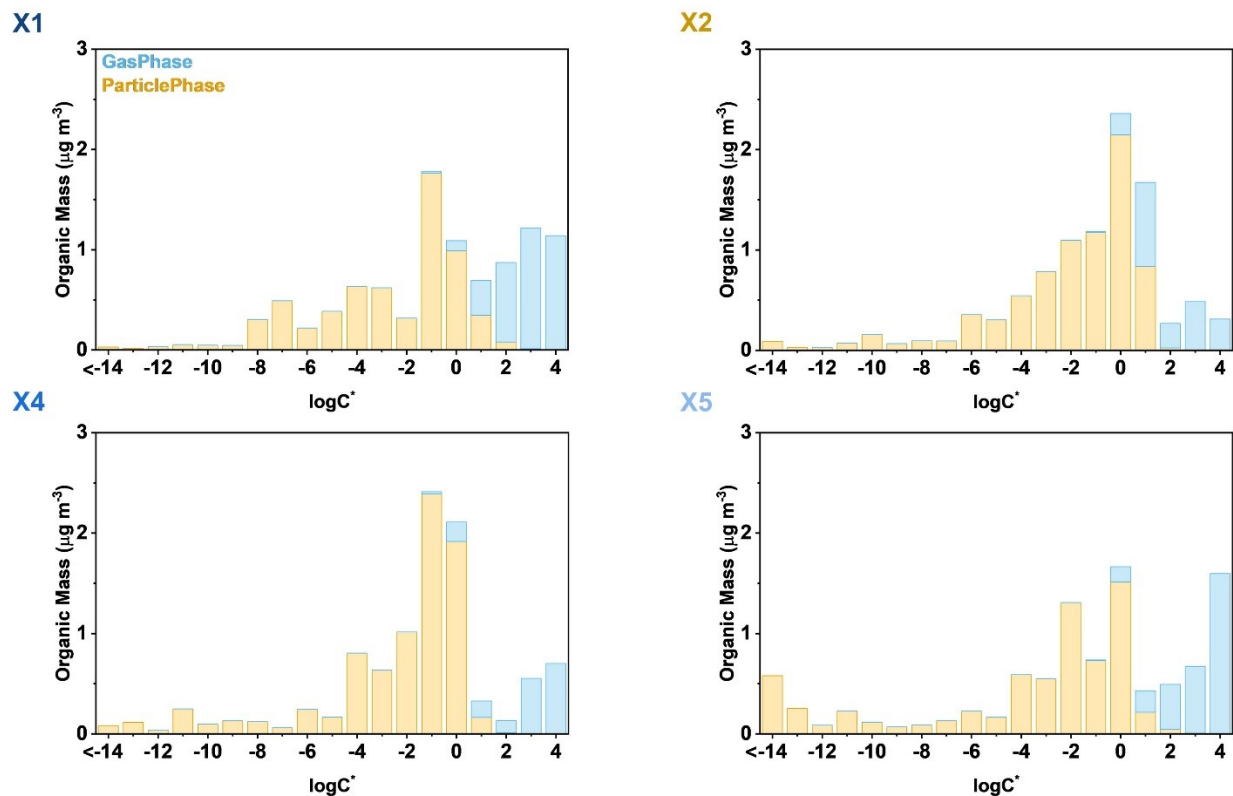


Figure S10. Volatility Basis Set (VBS) plots of organic components identified in the waste condensate samples, calculated for aerosolized mixtures with a total organic mass (OM) loading of $10 \mu\text{g m}^{-3}$. The estimated mass concentrations of individual components (C_i , $\mu\text{g m}^{-3}$) are binned into $\log C^*$ bins of integer values shown on the x-axis. Yellow and blue areas indicate OM fractions in particle and gas phases, respectively.

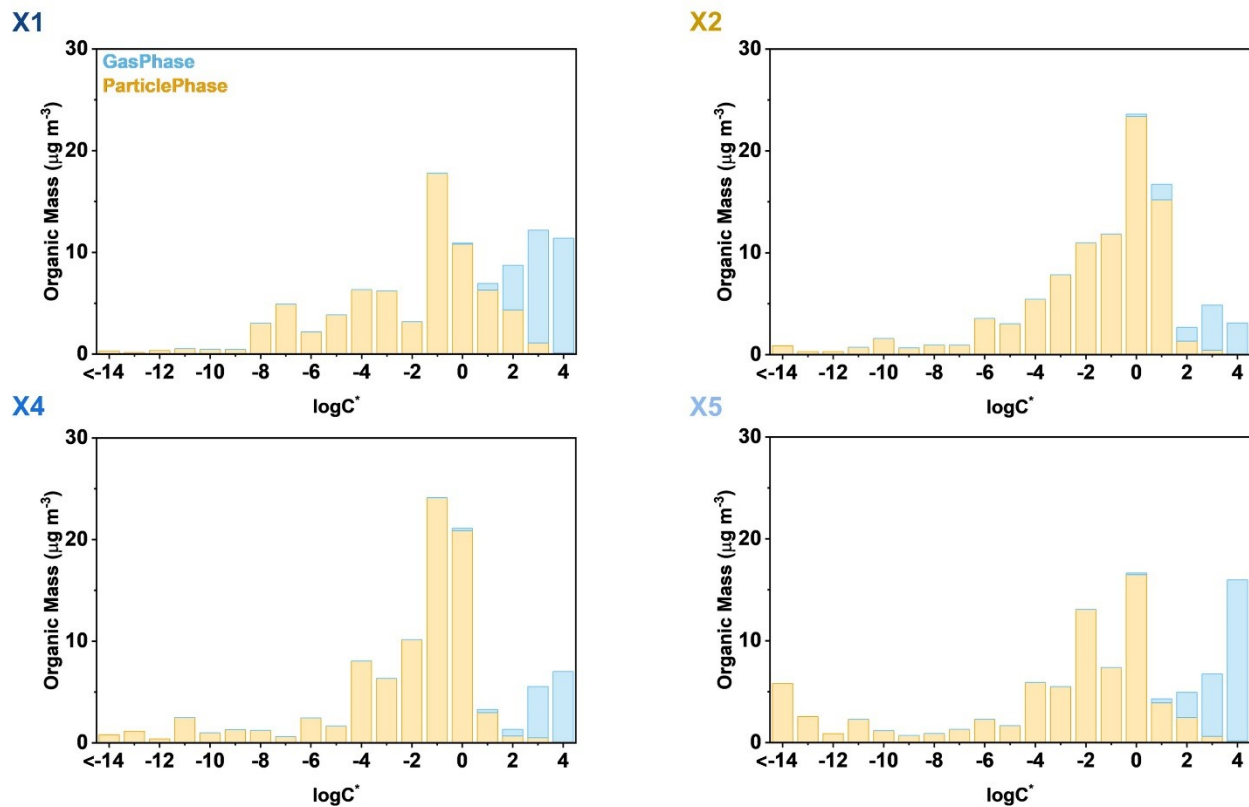


Figure S11. Volatility Basis Set (VBS) plots of organic components identified in the waste condensate samples, calculated for aerosolized mixtures with a total organic mass (OM) loading of $100 \mu\text{g m}^{-3}$. The estimated mass concentrations of individual components ($C_i, \mu\text{g m}^{-3}$) are binned into $\log C^*$ bins of integer values shown on the x-axis. Yellow and blue areas indicate OM fractions in particle and gas phases, respectively.

Supplementary Note 10: *Estimation of glass transition temperature and viscosity values of individual molecular components.*

Figure S12 shows the glass transition temperatures (T_g) used to estimate the viscosity of individual species. Figure S13 shows the estimated viscosity (η) as a function of molar mass for assigned species colored by their O:C ratio. It is important to note that the η was only determined for compounds in the CHO class based on the parameterization developed by DeRieux et al. (2018).³ Additionally, Figure S13 presents compounds with molar masses 80 g mol^{-1} to 450 g mol^{-1} due to the theoretical limits in the viscosity calculation.⁴ The colors of the figures correspond to the viscosity of liquids ($< 10^2 \text{ Pa s}$), semi-solids ($10^2 - 10^{12} \text{ Pa s}$), and amorphous glass solids ($> 10^{12} \text{ Pa s}$).¹⁶ Reference viscosities are also shown on Figure S13 for water (10^{-2} Pa s), olive oil (10^{-1} Pa s), honey (10^0 Pa s), ketchup (10^2 Pa s), peanut butter (10^3 Pa s), pitch (10^8 Pa s), and glass marbles (10^{12} Pa s). In Figure S13, the compounds with low O:C ratios are liquid-like, however the compounds with higher O:C ratios are more viscous across all the samples. Furthermore, 76% to 80% of the total number of assigned compounds contributed to the semi-solid or solid compound classes with viscosities equal to or higher than 10^2 Pa s , indicating this chemical mixture will have high viscosity.

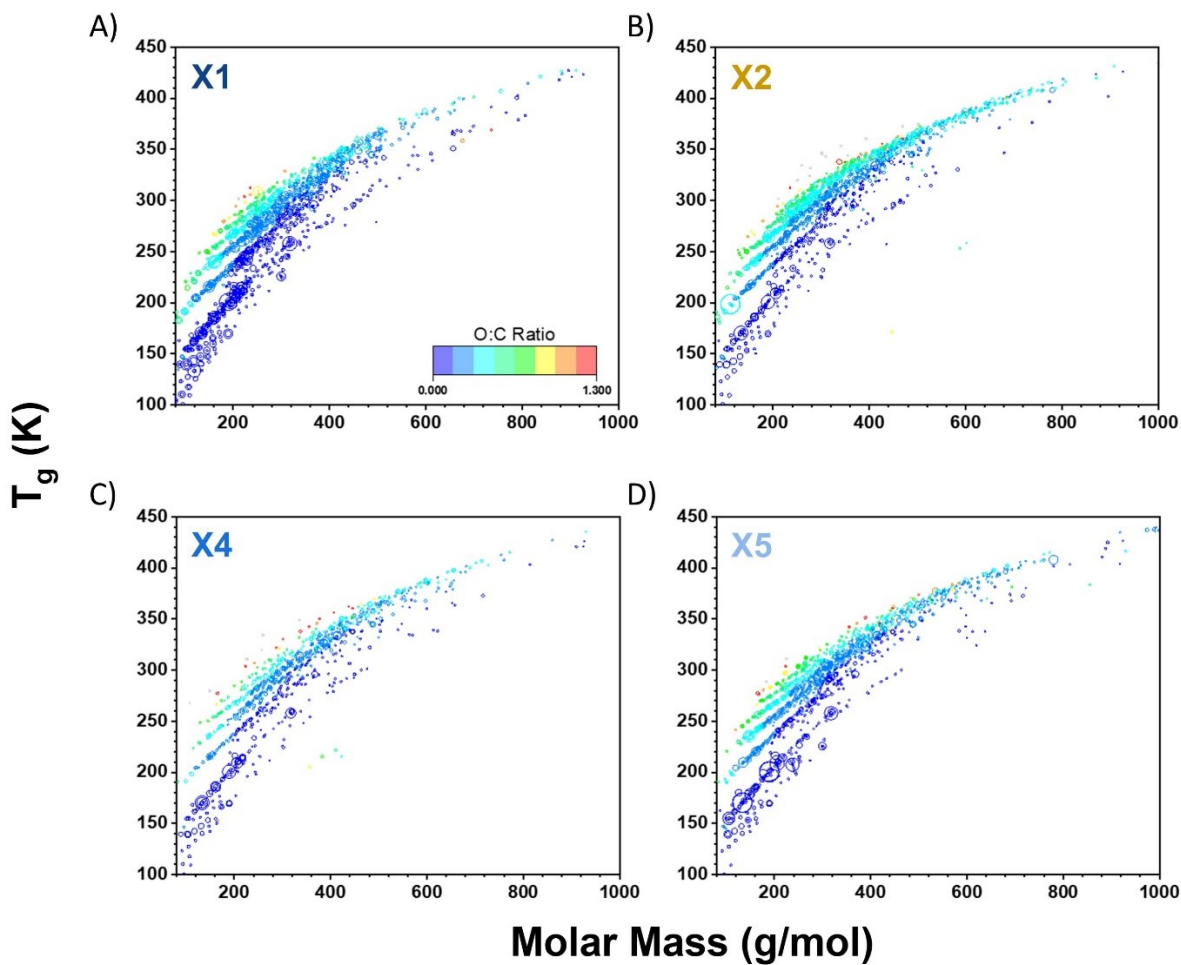


Figure S12. Glass transition temperature (T_g) as a function of molar mass. Sizes of individual symbols are proportional to the intensity^{1/4} of corresponding MS peaks. Colors of symbols are proportional to the oxygen to carbon ratio of the neutral formulas in both APPI and ESI modes.

Fi

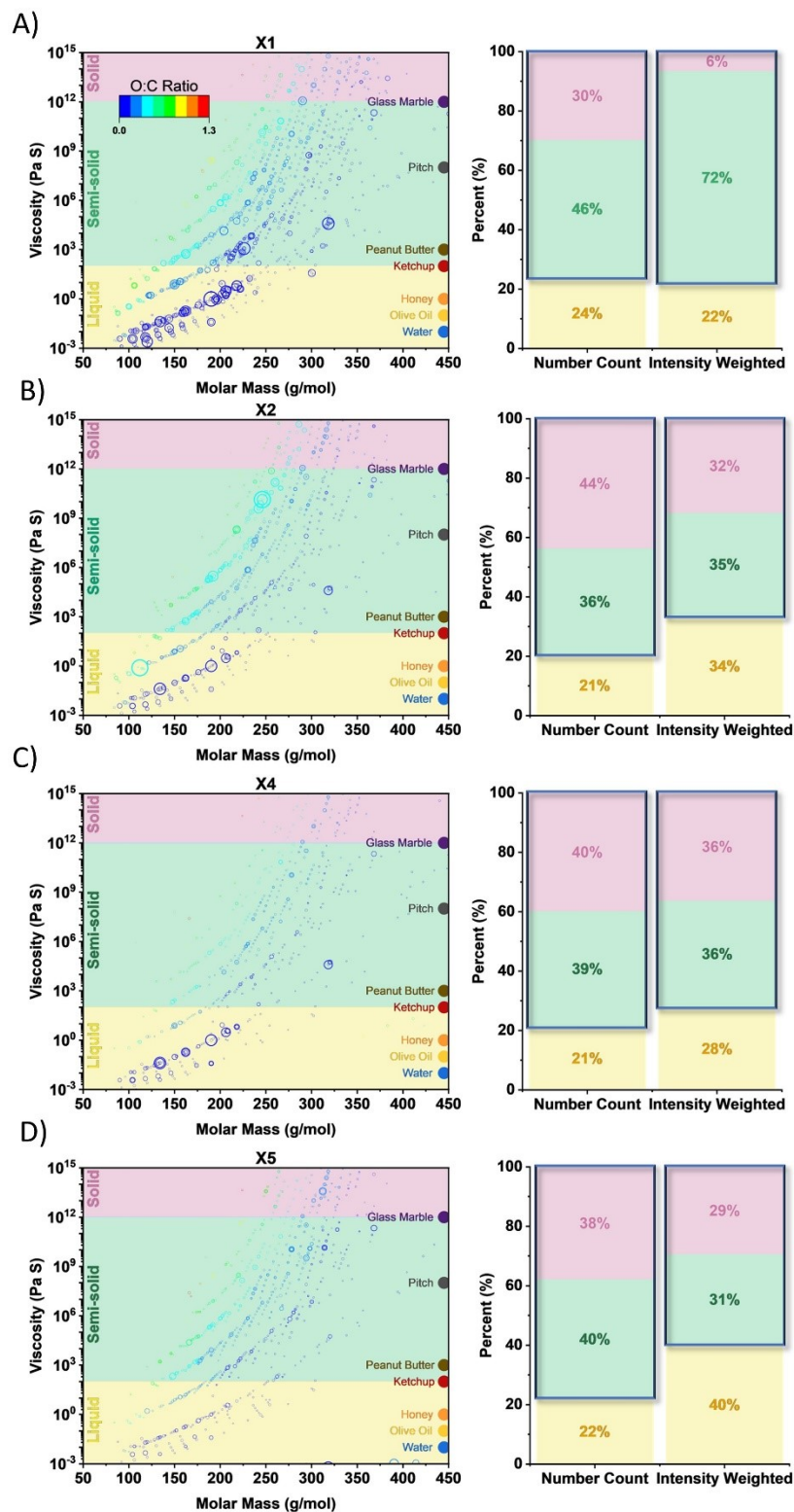


Figure S13. Predicted viscosity of species in each CIPP waste condensate as a function of molar mass. Sizes of individual symbols are proportional to the intensity^{1/4} of corresponding MS peaks. Colors of

symbols are proportional to the oxygen to carbon ratio of the neutral formulas in both APPI and ESI modes. The background colors indicate the viscosity ranges reported in Koop et al. (2011):¹⁶ from top to bottom, solid, semi-solid, and liquid. Reference viscosities are listed (from lowest to highest): water (blue; 10^{-2}), olive oil (olive oil; 10^{-1}), honey (orange; 10^0), ketchup (red; 10^2), peanut butter (brown; 10^3), pitch (black; 10^8), and glass marbles (purple; 10^{12}). Percent contribution of counts and MS intensity of assigned species to viscosity class for each CIPP waste condensate are presented on the right side of each viscosity plot. Blue boxes represent solid and semi-solid fractions that will contribute to SOA mass.

Supplementary Note 11: *Calibration curves and optical features for selected quantified species.*

Calibration curves were constructed using HPLC-PDA-HRMS analysis of commercial standards all purchased from Millipore Sigma. Specifically, benzoic acid (>99%), methyl methacrylate (99%), benzaldehyde ($\geq 99\%$), acetophenone (>99%), tripropylene glycol diacrylate ($\geq 82.5\%$), and dibutyl phthalate ($\geq 98\%$). Analysis of the standards employed same separation method described in the main manuscript. EIC peak areas were used to construct calibration curves over the range of 0.5 - 100 ng of injected mass loadings (Figure S14). Most of these species strongly absorb UV light (Figure S15). However, the PDA features were not used for quantitation because not all selected standards absorbed light, and the retained features were difficult to distinguish from the complex condensate mixtures as a result of coeluting components.

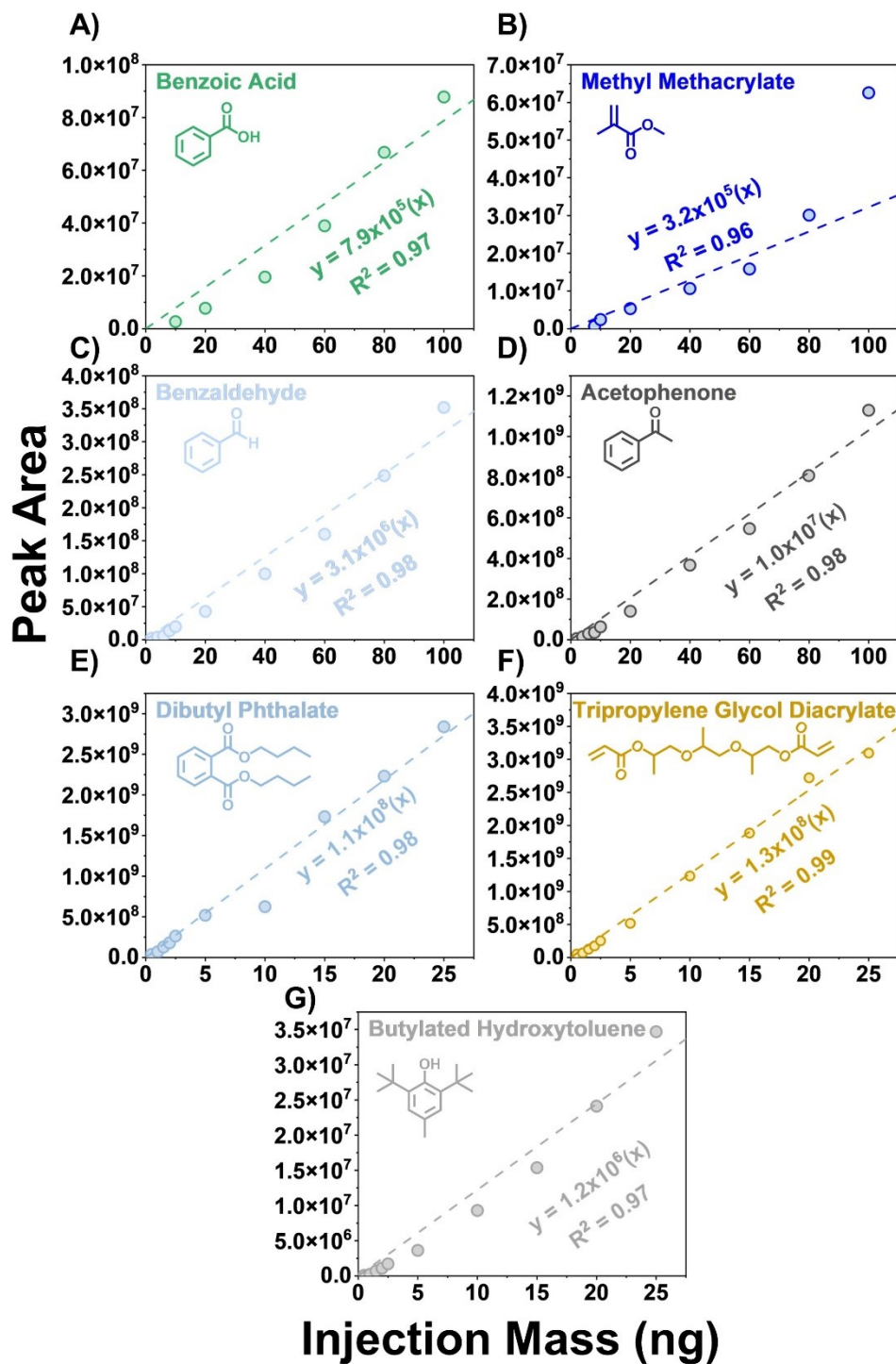


Figure S14. Calibration curves used for quantitation of selected components based on EIC peak area. Six- or eight-point calibration curves were constructed by separating and injecting known concentrations of each standard using the HPLC-PDA-ESI-HRMS setup. All standards were investigated in ESI(+) mode, except butylated hydroxytoluene, which is only ionizable in ESI(-) mode. The number of points on the calibration curve was determined using the limit of detection for each standard. Methyl methacrylate calibration was conducted excluding the outlier point in the top right of the panel B.

Table S2. Limits of detection and quantitation for the selected resin components quantified.

	Limit of Detection (mg L ⁻¹)	Limit of Quantitation (mg L ⁻¹)
Benzoic acid	2.15×10^{-7}	7.17×10^{-7}
Methyl methacrylate	6.79×10^{-7}	2.26×10^{-6}
Benzaldehyde	3.24×10^{-8}	1.05×10^{-7}
Acetophenone	7.76×10^{-9}	2.59×10^{-8}
Tripropylene glycol diacrylate	8.42×10^{-11}	2.81×10^{-10}
Dibutyl phthalate	2.08×10^{-10}	6.94×10^{-10}
Butylated hydroxytoluene	2.29×10^{-8}	7.63×10^{-8}

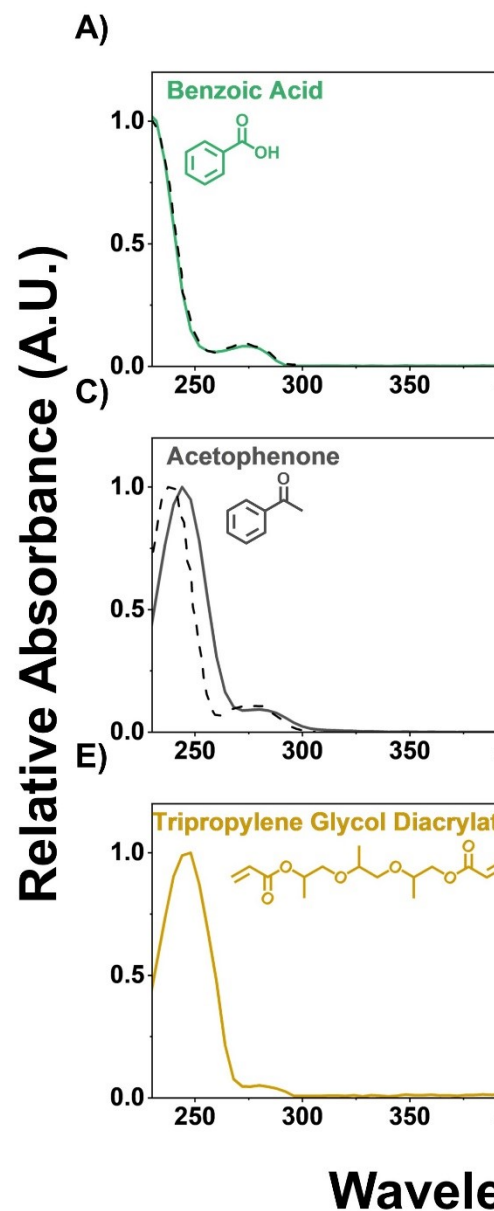


Figure S15. *UV-vis spectra of selected resin components based on PDA detection.* UV-vis spectra were obtained based on the peak in the PDA chromatogram using the highest concentration calibration sample. Methyl methacrylate did not have an apparent PDA feature; therefore, it is excluded from this figure. Reference spectra from literature are included as dashed lines.¹⁷⁻²¹

Supplementary Note 12: References.

- (1) Li, Y.; Pöschl, U.; Shiraiwa, M. Molecular Corridors and Parameterizations of Volatility in the Chemical Evolution of Organic Aerosols. *Atmospheric Chem. Phys.* **2016**, *16* (5), 3327–3344. <https://doi.org/10.5194/acp-16-3327-2016>.
- (2) Donahue, N. M.; Trump, E. R.; Pierce, J. R.; Riipinen, I. Theoretical Constraints on Pure Vapor-Pressure Driven Condensation of Organics to Ultrafine Particles: Organic Condensation. *Geophys. Res. Lett.* **2011**, *38* (16), n/a-n/a. <https://doi.org/10.1029/2011GL048115>.
- (3) DeRieux, W.-S. W.; Li, Y.; Lin, P.; Laskin, J.; Laskin, A.; Bertram, A. K.; Nizkorodov, S. A.; Shiraiwa, M. Predicting the Glass Transition Temperature and Viscosity of Secondary Organic Material Using Molecular Composition. *Atmospheric Chem. Phys.* **2018**, *18* (9), 6331–6351. <https://doi.org/10.5194/acp-18-6331-2018>.
- (4) Angell, C. A. Relaxation in Liquids, Polymers and Plastic Crystals — Strong/Fragile Patterns and Problems. *J. Non-Cryst. Solids* **1991**, *131–133*, 13–31. [https://doi.org/10.1016/0022-3093\(91\)90266-9](https://doi.org/10.1016/0022-3093(91)90266-9).
- (5) Kroll, J. H.; Donahue, N. M.; Jimenez, J. L.; Kessler, S. H.; Canagaratna, M. R.; Wilson, K. R.; Altieri, K. E.; Mazzoleni, L. R.; Wozniak, A. S.; Bluhm, H.; Mysak, E. R.; Smith, J. D.; Kolb, C. E.; Worsnop, D. R. Carbon Oxidation State as a Metric for Describing the Chemistry of Atmospheric Organic Aerosol. *Nat. Chem.* **2011**, *3* (2), 133–139. <https://doi.org/10.1038/nchem.948>.
- (6) Kroll, J. H.; Lim, C. Y.; Kessler, S. H.; Wilson, K. R. Heterogeneous Oxidation of Atmospheric Organic Aerosol: Kinetics of Changes to the Amount and Oxidation State of Particle-Phase Organic Carbon. *J. Phys. Chem. A* **2015**, *119* (44), 10767–10783.
- (7) Lv, J.; Zhang, S.; Luo, L.; Cao, D. Solid-Phase Extraction-Stepwise Elution (SPE-SE) Procedure for Isolation of Dissolved Organic Matter Prior to ESI-FT-ICR-MS Analysis. *Anal. Chim. Acta* **2016**, *948*, 55–61.
- (8) Tao, S.; Lu, X.; Levac, N.; Bateman, A. P.; Nguyen, T. B.; Bones, D. L.; Nizkorodov, S. A.; Laskin, J.; Laskin, A.; Yang, X. Molecular Characterization of Organosulfates in Organic Aerosols from Shanghai and Los Angeles Urban Areas by Nanospray-Desorption

- Electrospray Ionization High-Resolution Mass Spectrometry. *Environ. Sci. Technol.* **2014**, *48* (18), 10993–11001. <https://doi.org/10.1021/es5024674>.
- (9) Koch, B. P.; Dittmar, T. From Mass to Structure: An Aromaticity Index for High-Resolution Mass Data of Natural Organic Matter. *Rapid Commun. Mass Spectrom.* **2006**, *20* (5), 926–932. <https://doi.org/10.1002/rcm.2386>.
- (10) Koch, B. P.; Dittmar, T. From Mass to Structure: An Aromaticity Index for High-Resolution Mass Data of Natural Organic Matter. *Rapid Commun. Mass Spectrom.* **2016**, *30* (1), 250–250. <https://doi.org/10.1002/rcm.7433>.
- (11) Kim, S.; Kramer, R. W.; Hatcher, P. G. Graphical Method for Analysis of Ultrahigh-Resolution Broadband Mass Spectra of Natural Organic Matter, the Van Krevelen Diagram. *Anal. Chem.* **2003**, *75* (20), 5336–5344. <https://doi.org/10.1021/ac034415p>.
- (12) Lobodin, V. V.; Marshall, A. G.; Hsu, C. S. Compositional Space Boundaries for Organic Compounds. *Anal. Chem.* **2012**, *84* (7), 3410–3416. <https://doi.org/10.1021/ac300244f>.
- (13) Donahue, N. M.; Kroll, J. H.; Pandis, S. N.; Robinson, A. L. A Two-Dimensional Volatility Basis Set–Part 2: Diagnostics of Organic-Aerosol Evolution. *Atmospheric Chem. Phys.* **2012**, *12* (2), 615–634.
- (14) Donahue, N. M.; Robinson, A. L.; Pandis, S. N. Atmospheric Organic Particulate Matter: From Smoke to Secondary Organic Aerosol. *Atmos. Environ.* **2009**, *43* (1), 94–106. <https://doi.org/10.1016/j.atmosenv.2008.09.055>.
- (15) Nguyen, T. B.; Nizkorodov, S. A.; Laskin, A.; Laskin, J. An Approach toward Quantification of Organic Compounds in Complex Environmental Samples Using High-Resolution Electrospray Ionization Mass Spectrometry. *Anal. Methods* **2013**, *5* (1), 72–80. <https://doi.org/10.1039/C2AY25682G>.
- (16) Koop, T.; Bookhold, J.; Shiraiwa, M.; Pöschl, U. Glass Transition and Phase State of Organic Compounds: Dependency on Molecular Properties and Implications for Secondary Organic Aerosols in the Atmosphere. *Phys. Chem. Chem. Phys.* **2011**, *13* (43), 19238. <https://doi.org/10.1039/c1cp22617g>.
- (17) Karimova, N. V.; Luo, M.; Grassian, V. H.; Gerber, R. B. Absorption Spectra of Benzoic Acid in Water at Different PH and in the Presence of Salts: Insights from the Integration of Experimental Data and Theoretical Cluster Models. *Phys. Chem. Chem. Phys.* **2020**, *22* (9), 5046–5056. <https://doi.org/10.1039/C9CP06728K>.

- (18) Kawamura, K.; Yasuda, T.; Hatanaka, T.; Hamahiga, K.; Matsuda, N.; Ueshima, M.; Nakai, K. Oxidation of Aliphatic Alcohols and Benzyl Alcohol by H₂O₂ under the Hydrothermal Conditions in the Presence of Solid-State Catalysts Using Batch and Flow Reactors. *Chem. Eng. J.* **2016**, *285*, 49–56. <https://doi.org/10.1016/j.cej.2015.09.088>.
- (19) Thomas, O.; Brogat, M. Organic Constituents. In *UV-Visible Spectrophotometry of Water and Wastewater*; Elsevier, 2017; pp 73–138. <https://doi.org/10.1016/B978-0-444-63897-7.00003-2>.
- (20) Capobianco, A.; Caruso, T.; Palombi, L.; Peluso, A. Detection of an Ylide Intermediate in the Electrochemically-Induced Stevens Rearrangement of an Ammonium Salt by in Situ UV–Vis Spectroelectrochemistry. *Electrochimica Acta* **2013**, *92*, 446–451. <https://doi.org/10.1016/j.electacta.2013.01.079>.
- (21) Fihtengolts, V. Atlas of UV Absorption Spectra of Substances Used in Synthetic Rubber Manufacture. *NIST Chem. WebBook NIST Stand. Ref. Database* **1969**, 69.